

Luminous dark matterBrian Feldstein,¹ Peter W. Graham,² and Surjeet Rajendran³¹*Department of Physics, Boston University, Boston, Massachusetts 02215, USA*²*Department of Physics, Stanford University, Stanford, California 94305*³*Center for Theoretical Physics, Laboratory for Nuclear Science and Department of Physics, Massachusetts Institute of Technology, Cambridge, Massachusetts 02139, USA*

(Received 19 August 2010; published 29 October 2010)

We propose a dark matter model in which the signal in direct detection experiments arises from electromagnetic, not nuclear, energy deposition. This can provide a novel explanation for the DAMA result while avoiding many direct detection constraints. The dark matter state is taken nearly degenerate with another state. These states are naturally connected by a dipole moment operator, which can give both the dominant scattering and decay modes between the two states. The signal at DAMA then arises from dark matter scattering in the Earth into the excited state and decaying back to the ground state through emission of a single photon in the detector. This model has unique signatures in direct detection experiments. The density and chemical composition of the detector is irrelevant—only the total volume affects the event rate. In addition, the spectrum is a monoenergetic line, which can fit the DAMA signal well. This model is readily testable at experiments such as CDMS and XENON100 if they analyze their low-energy, electronic recoil events.

DOI: [10.1103/PhysRevD.82.075019](https://doi.org/10.1103/PhysRevD.82.075019)

PACS numbers: 95.35.+d

I. INTRODUCTION AND OVERVIEW

The signal in DAMA is now highly statistically significant [1,2]. However, the interpretation is still unclear. The constraints from many other direct detection experiments, including CDMS [3] and XENON100 [4], rule out the simplest interpretation in terms of a weakly interacting massive particle (WIMP) elastically scattering off nuclei. Of course, comparing these different experimental constraints is highly model-dependent and indeed several models have been put forward to explain the positive signal in DAMA while avoiding other direct detection constraints including inelastic dark matter (IDM) [5], exothermic dark matter [6], form factor dark matter [7–9], resonant dark matter [10], and light dark matter [11–13]. All these models rely on nuclear scattering in DAMA to explain their signal. We wish to propose a different explanation.

Many models beyond the standard model have several states, of which one (or more) is stable and thus makes up the dark matter of our Universe. It is natural for these states to be mixed by a dipole moment operator. Such operators are induced by loops in many theories including supersymmetry. Although the dipole moment operator may be avoided, it seems generic to consider the possibility that it exists at some level. We will then make one further assumption, that the mass splitting between the dark matter state and another state in the spectrum is small, \sim keV. Many models that explain the DAMA results make use of such small mass splittings. We will argue that these assumptions, two nearly degenerate states connected by a dipole moment operator, can explain the DAMA results by electronic instead of nuclear scattering events, thus avoiding the constraints from most other direct detection

experiments. DAMA is one of the only direct detection experiments that does not attempt to veto electronic events.

Because the splitting is small and the dipole moment is a higher dimension operator suppressed, for example, by \sim TeV, the excited state of dark matter can actually live for a significant amount of time. This means that, just due to the dipole moment operator, dark matter will upscatter into the excited state in the Earth and then decay back to the ground state a significant distance away. These decays happen by single photon emission and thus when they happen in a detector will appear as an electromagnetic, not nuclear, scattering. As explained more completely in Sec. II, the decay rate per unit volume in the Earth is naturally close to the original nuclear scattering rate and thus of the right order to explain the DAMA result. Note that this explanation is quite different from recently proposed models which involve a dipole moment induced nuclear scattering [14–16].

Generally, electronic scattering has not worked as an explanation for the DAMA result due to the large form factor that suppresses the scattering of a heavy WIMP off a light electron [17]. Alternatively, absorbing light axionlike dark matter leads to a very low annual modulation [18]. Our model avoids such problems because the dark matter does not actually scatter off electrons. Instead it produces a photon which then easily dumps all its energy in the detector. Because the dark matter is slow, the photons produced are monoenergetic and appear as a line spectrum in a detector. Interestingly, a line, smeared by DAMA's energy resolution, fits the DAMA signal well. In fact, more generally than explaining the DAMA result, this model can produce electron-recoil events instead of nuclear-recoil events without a large form factor suppression.

II. LUMINOUS DARK MATTER

In its most general form, the scenario we are considering requires two components: First, we require an interaction to mediate an inelastic scattering of the dark matter particle within the Earth, up to a higher energy state, and second, we require an interaction leading to a decay of this higher energy state into a set of products which includes photons. Of course, it is also necessary to ensure that the interactions available do not also lead to unacceptably fast decays of the original dark matter particle.

Here we will concentrate on a simple scenario in which all of the requirements are satisfied by a single dark sector interaction term. In particular, we will take an interaction which results from the magnetic dipole moment operator

$$\mathcal{L}_M = \frac{i}{4\Lambda} \bar{\chi}_g \sigma^{\mu\nu} \chi_e F_{\mu\nu} + \text{H.c.}, \quad (1)$$

where here χ_g and χ_e are two distinct fermions, which we will take to be Majorana for simplicity. We will discuss a straightforward mechanism leading to such an interaction in Sec. II B.¹

We will take the dark matter particle to be χ_g , and to have a mass $m_{\chi} \sim 1$ GeV, while χ_e will have a mass which is higher than this by a splitting δ of size 3.3 keV, chosen to fit the observed DAMA spectrum. The light dark matter masses we employ will be heavy enough to allow for sufficient kinetic energy for upscattering, while also being light enough to allow the required cross sections to evade current direct detection limits; the nuclear-recoil events simply deposit too little energy to have been seen by present dark matter searches. The photon decay products, on the other hand, lead to various constraints on the model which will be discussed in detail in Sec. III.

After the dark matter particle has upscattered in the Earth to the higher energy state, the resulting particle may travel a great distance before ultimately decaying. Note that there is no need for both processes to occur within the DAMA detector. Indeed, if the typical travel distance before the decay is less than roughly the Earth's radius, then, with the cross section fixed, the signal at DAMA is actually independent of the decay rate. This is easy to understand, since the upscatter and decay events are then spread roughly evenly throughout the Earth, and thus automatically have comparable rates per unit volume, on average. Indeed, this regime will apply throughout the viable parameter space of the model. Note that a 3.3 keV line gives an excellent fit to the spectrum observed at DAMA, due to the energy resolution of the detectors of about 0.8 keV at this energy scale [19]. A comparison

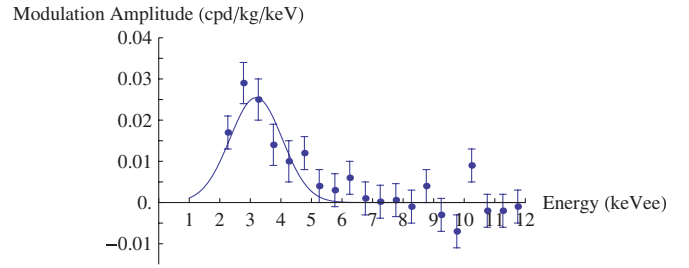


FIG. 1 (color online). A comparison of the predicted and observed spectra at DAMA for a line at 3.3 keV using the assumptions defined in the text. The dots represent the DAMA data points, while the line is an example of a fit from our model.

between the observed and predicted spectra is shown in Fig. 1.

Before proceeding to the calculation of the event rate at DAMA, let us briefly consider some of the key similarities and differences between this scenario and the usual case of inelastic dark matter. In the inelastic dark matter scenario, interactions mediating elastic scattering are required to be significantly suppressed compared to the dominant inelastic interactions. If this were not the case, the elastic interactions would lead to unacceptably large signals at direct detection experiments. In the present model, however, the constraints on the elastic scattering cross section are much weaker; indeed, there is no problem having elastic cross sections of the same order as the inelastic ones.² An important feature which our scenario has in common with inelastic dark matter, on the other hand, lies in the possibility for the existence of a boost to the annual modulation fraction. At the small masses we consider, only dark matter particles on the rapidly falling tail of the halo velocity distribution have sufficient kinetic energy to upscatter, leading to the boost. For standard WIMPs, this would lead to an unsuitably sharp spectrum at DAMA, but in both our scenario and IDM, this problem is solved by the details of the mechanism; in IDM the spectrum is fixed by the cutoff in available low-energy phase-space, while in our model the spectrum is fixed due to its origin in the monochromatic photon decay. This boost to the annual modulation fraction is needed due to the bounds on a purely electromagnetic signal at the XENON100 experiment [4] (and to a lesser extent, the CDMS experiment). As will be discussed further in Sec. III, we require modulation fractions larger than around 50%, and this will constrain from above the masses for which our scenario is viable.

We now turn to a calculation of the event rate at DAMA. In principle, this calculation is made quite complicated by the angular dependence of the inelastic dipole scattering cross section. Events leading to a signal at DAMA must

¹We assume that CP is a good enough symmetry in the dark sector so as to sufficiently suppress a possible electric dipole moment operator, which would otherwise be the dominant channel for scattering due to a $1/v^2$ enhancement.

²Note on the other hand that a magnetic dipole interaction could not mediate elastic scattering of our Majorana dark matter particle, since such an interaction would vanish by fermion anticommutation.

involve dark matter particles upscattered within the Earth toward the direction of the experiment. The probability for this to occur depends on the relative locations in the Earth of the initial upscattering event and the DAMA detector, as well as on the orientation of the incoming dark matter velocity. A complete calculation of the predicted rate at DAMA is therefore fairly complicated, and in practice is rather time-consuming to perform numerically. As a result we will content ourselves with calculating the expected event rate—and required cross sections—to within a factor of ~ 4 , and will make a number of simplifying approximations. The number of events we predict to have been seen at XENON100 follows directly from the DAMA event rate, and the given modulation fraction. Since the modulation fraction is essentially fixed by the dark matter mass and not the overall cross section, the severity of the XENON100 constraint is essentially independent of any uncertainty introduced through our approximations. The other main constraint on our model comes from the SWIFT x-ray satellite [20], and will be discussed further in Sec. III. Generally, the approximations we make should tend to underestimate the required cross sections and decay rates slightly, thus making the SWIFT constraint appear a bit stronger than it otherwise might; faster decay rates result in fewer χ_e particles reaching the height of the satellite. Note, however, that uncertainty in the composition of the Earth could affect the SWIFT constraint in either direction.

The approximations we will make are as follows:

- (1) We will take the Earth to have radius $r_\oplus = 6.4 \times 10^6$ m, and to consist of a uniform crust of density 2.9 g/cm^3 and depth 40 km, and a mantle region with density increasing linearly with depth from 3.3 g/cm^3 to 5.7 g/cm^3 . The Earth's core will be taken to be a uniform sphere with radius 3500 km and density 10.5 g/cm^3 . Note however that for the viable parameter space of our model, the typical distances travelled by upscattered dark matter particles before they decay is on the order of 100–1000 km, and thus upscattering in the core does not actually contribute to the signal. The elemental abundances we take for each section of the Earth are given in Table I.³ It should be kept in mind that we do not actually know the specific elemental abundances to be found in the vicinity of the DAMA experiment, and so we simply take typical values.⁴
- (2) In determining the scattering cross sections and kinematics for upscattering, we will approximate all relevant elements in the Earth as being infinitely heavy compared to the dark matter particle. More realistically, scattering from lighter elements, especially oxygen, would be suppressed or even

TABLE I. The elemental abundances of the Earth assumed for our calculations, obtained from [21].

Element	Crust abundance	Mantle abundance	Core abundance
	by mass	by mass	by mass
O	46%	45%	0%
Mg	3%	23%	0%
Al	9%	2%	0%
Si	29%	22%	6%
Ca	4%	2%	0%
Fe	5%	6%	86%

kinematically forbidden. However, we estimate the error introduced in this way to be less than about a factor of 2.⁵ This will result in the important simplification that the upscattered dark matter velocity will be independent of the scattering angle.

- (3) We will work with upscattering cross sections which have been integrated over angles, rather than with the true angular dependent differential cross sections. We estimate that this approximation will introduce an error of less than about a factor of 2. Note that the true cross sections are in fact angular independent at the threshold for upscattering. Beyond threshold, on the other hand, they quickly become fairly forward peaked. The reason our approximation is a good one, is that the falling halo velocity distribution results in most upscattering events taking place quite close to threshold.

With these approximations in hand, calculating the event rate at DAMA is straightforward. The total rate per unit detector mass is given by

$$\mathcal{R} = \frac{\rho_{\text{DM}}}{m_\chi \rho_{\text{NaI}}} \sum_i \int d^3 \vec{v} f(\vec{v}) \int_{\text{Earth}} d^3 \vec{r} n_i(\vec{r}) \sigma_i v \mathcal{P}(\vec{r}, v). \quad (2)$$

Here $f(\vec{v})$ is the dark matter velocity distribution in the Earth frame, which we will take to have the standard form

$$f(\vec{v}) = \frac{1}{(\pi \bar{v}^2)^{3/2}} e^{-(\vec{v} + \vec{v}_e)^2 / \bar{v}^2} \Theta(v_{\text{esc}} - |\vec{v} + \vec{v}_e|), \quad (3)$$

with a cutoff in the Galactic frame at $v_{\text{esc}} = 650 \text{ km/s}$.⁶ We will take \bar{v} to be 220 km/s and the Galactic speed of Earth v_e to be $232 \text{ km/s} + 15 \cos(2\pi(t - t_0)) \text{ km/s}$, with $t_0 = \text{June 2nd}$ and t in years. ρ_{DM} is the local dark matter density, which we will set to 0.3 GeV/cm^3 , and ρ_{NaI} is the sodium iodide density of 3.67 g/cm^3 . σ_i is the total cross section to upscatter from a given element i , with i running over the rows of Table I, and $n_i(\vec{r})$ is the number density distribution in the Earth for the given element. $\mathcal{P}(\vec{r}, v)$ is

³We ignore various elements with small abundances.

⁴Note that since both DAMA and XENON100 are located in the Gran Sasso mine, the relative signals seen by these experiments are not influenced by this approximation.

⁵Indeed the changes that result from this approximation can be compensated for by making a small adjustment to the dark matter mass.

⁶Taking $v_{\text{esc}} = 600 \text{ km/s}$ would simply shift the required mass range slightly.

the probability that an upscattering event in the Earth at position \vec{r} with incoming speed v leads to a decay within the DAMA dark matter detector, divided by the detector volume. After upscattering, the excited state moves with speed $v_f = \sqrt{v^2 - 2\frac{\delta}{m_\chi}}$, so that we have

$$\mathcal{P}(\vec{r}, v) = \frac{1}{4\pi(\vec{r} - \vec{r}_{\text{DAMA}})^2} \frac{\Gamma}{v_f} e^{-\Gamma|\vec{r} - \vec{r}_{\text{DAMA}}|/v_f}, \quad (4)$$

with r_{DAMA} being the position in the Earth of the detector.

$$\frac{d\sigma_M}{d\Omega} = \frac{e^2 Z^2 [\delta^2 m_\chi^2 - 4\delta m_\chi^3 v^2 + 2m_\chi^4 v^4 - 2m_\chi^2 v v_f (m_\chi^2 v^2 - \delta m_\chi) \cos(\theta)]}{16\pi^2 \Lambda^2 [\delta m_\chi - m_\chi^2 v^2 + m_\chi^2 v v_f \cos(\theta)]^2}, \quad (5)$$

which after integrating over angles becomes

$$\sigma_M = \frac{e^2 Z^2 [2(m_\chi v^2 - \delta) \tanh^{-1}(\frac{m_\chi v v_f}{m_\chi v^2 - \delta}) - m_\chi v v_f]}{4\pi \Lambda^2 m_\chi v v_f}. \quad (6)$$

Note that for all elements of interest, and for m_χ in the desired range, dipole-charge scattering always dominates over dipole-dipole scattering. Nuclear form factors are irrelevant due to the small momentum transfers present in our scattering events. The decay rate of the excited state χ_e is

$$\Gamma = \frac{1}{\pi \Lambda^2} \delta^3. \quad (7)$$

The available parameter region in the m_χ, Λ plane is plotted in Fig. 2. The thick purple diagonal stripe shows the parameter space which reproduces the correct rate at DAMA at 90% confidence, comparing with the lowest 8 points in the DAMA energy spectrum, using a 3.3 keV mass splitting. Note that the vertical thickness of this region is essentially set by the accuracy of the measurement of the DAMA event rate. The shaded blue triangle in the lower right (blue dashed line) shows the 90% confidence XENON100 constraint, which we have obtained by comparing the number of observed and predicted events within 1 standard deviation of energy resolution from the predicted peak. We apply Poisson statistics to the number of S1 photoelectrons produced in an event to obtain the energy resolution (XENON100 claims a light yield of 2.2 photoelectrons/keV). We use the energy-dependent acceptance plotted in Fig. 3 of [4], although we should note that this acceptance is actually that for nuclear recoils (before cuts from the S2 signal). No acceptance for electromagnetic events has been published by the XENON100 Collaboration at the present time, although the two acceptances are expected to be similar [22]. The red region in the upper right (red dashed line) shows the constraint from the measurements of the x-ray background by the SWIFT satellite, and will be discussed further in Sec. III. The horizontal thin yellow line shows the parameter points which produce the correct thermal relic density.

We calculated the results for Eq. (2) numerically, extracted the amplitude of the annual modulation, and can then compare with the measured rate at DAMA.

A. Results

For the magnetic dipole operator [1], the leading order differential cross section (in the center-of-mass frame) on a heavy element of atomic number Z is

which produce the correct thermal relic density. It is an appealing feature of luminous dark matter that the thermal relic density turns out to be roughly the correct size, simply from the requirement of meeting all of the other experimental constraints. Note that the uncertainty at the factor of ~ 4 level in our cross-section calculation will not spoil this statement; small changes to the assumed dark matter halo velocity distribution could be made in order to maintain the successful relic density if necessary.

Given the allowed range of values for Λ shown in the figure, the charge scattering cross section per proton in a given nucleus ranges from about 10^{-38} cm^2 to about 10^{-36} cm^2 .

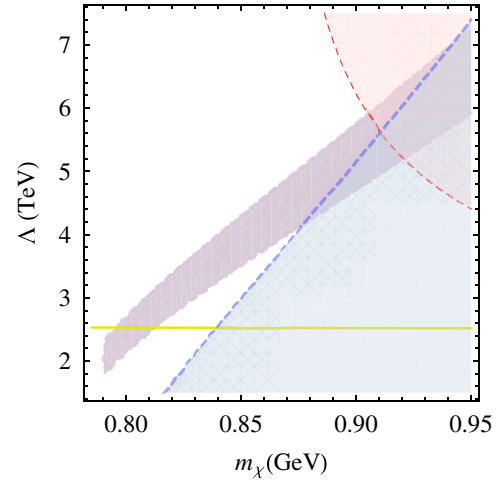


FIG. 2 (color online). The parameter space available to fit the DAMA signal at 90% confidence, using halo assumptions defined in the text and a 3.3 keV mass splitting. The vertical thickness of the allowed region (shaded region without boundary lines) is essentially fixed by the measured DAMA rate. The shaded triangular region in the lower right shows the 90% confidence XENON100 constraint, according to the assumptions defined in the text. The semicircular region in the upper right gives the x-ray background constraint from the SWIFT satellite. The solid, horizontal line shows the parameter points which produce the correct thermal relic density.

B. Generating inelastic dipole interactions

Constructing models which lead to interactions of the form [1] is straightforward. Essentially, we only need a few ingredients: first, a Dirac fermion

$$\psi = \begin{pmatrix} \psi_{L_1} \\ i\sigma_2 \psi_{L_2}^* \end{pmatrix}$$

with a ~ 1 GeV Dirac mass; second, a 3.3 keV Majorana mass for one of the two components of ψ , say ψ_{L_2} ; and third, a magnetic dipole interaction for ψ . This dipole interaction could arise, for example, from integrating out a heavy Dirac fermion and a heavy scalar, each carrying hypercharge, and with a Yukawa coupling to ψ . In general, magnetic dipole interactions are CP conserving, and may arise in many models after integrating out heavy particles. In the present scenario, the mass eigenstate fields are, at leading order, $\chi_{L_1} = \frac{i}{\sqrt{2}}(\psi_{L_1} - \psi_{L_2})$ and $\chi_{L_2} = \frac{1}{\sqrt{2}} \times (\psi_{L_1} + \psi_{L_2})$, with masses split by 3.3 keV. Writing

$$\chi_g = \begin{pmatrix} \chi_{L_1} \\ i\sigma_2 \chi_{L_1}^* \end{pmatrix}$$

and

$$\chi_e = \begin{pmatrix} \chi_{L_2} \\ i\sigma_2 \chi_{L_2}^* \end{pmatrix},$$

and expanding out the original dipole interaction for ψ , we obtain the inelastic dipole operator [1] as required.

III. CONSTRAINTS

In the scenario described in Sec. II, the dark matter consists of a single state χ_g with a mass m_χ . There is however another state χ_e , which is slightly heavier than χ_g by an amount $\delta \sim 2.5\text{--}3.5$ keV. The states χ_g and χ_e interact with the standard model through a magnetic dipole operator (1). As a result of this interaction, the dark matter χ_g can get upscattered to χ_e somewhere in the Earth. The subsequent decay $\chi_e \rightarrow \chi_g + \gamma$ can occur in a dark matter detector like DAMA's, producing a $\sim 2.5\text{--}3.5$ keV γ ray that appears in the electronic channel of the detector. With the parameters chosen in Sec. II, this decay explains the observed signal at DAMA, since DAMA analyzes both nuclear and electron-recoil events.

Both aspects of this scenario, the initial upscattering process and the decays of the excited state, are constrained by observations. We begin with the initial, upscattering process which dumps energy in dark matter detectors. Following this, we analyze decays of the excited state. We then briefly review collider and other astrophysical constraints on this scenario.

A. Upscattering

The dark matter χ_g interacts with nuclei through the operator (1). In this endothermic process, the kinetic energy $\sim m_\chi v^2$ of χ_g is partially consumed to provide the energy δ necessary to excite $\chi_g \rightarrow \chi_e$. The remaining kinetic energy $\sim m_\chi v^2 - \delta$ is shared between the kinetic energy of χ_e and the recoiling nucleus (of mass m_N). This scenario can explain the DAMA signal without running afoul of other experimental bounds only when $m_\chi \lesssim 1$ GeV (see Secs. II and III B 2). In this regime, $m_\chi \ll m_N$ and the energy carried away by the recoiling nucleus is $\sim \frac{m_\chi}{m_N} \delta \lesssim 0.10$ keV $(\frac{28 \text{ GeV}}{m_N})(\frac{\delta}{3 \text{ keV}})(\frac{m_\chi}{1 \text{ GeV}})$. These recoils are below the thresholds of current dark matter experiments [6].

However, as pointed out in [6], it is possible that a low threshold experiment like XENON10 could nevertheless place a bound on such subthreshold recoils due to upward fluctuations of photoelectron counts from such events. Similarly, a low threshold, light nucleus experiment like CDMS Silicon could also have some sensitivity to such events, after accounting for detector efficiencies at such low recoil energies. The single nucleon upscattering cross sections required to explain the DAMA events in this scenario are $\sim 10^{-36}\text{--}10^{-38}$ cm² (see Sec. II). These cross sections were found to be safe from the above considerations for light dark matter in [6]. In particular, the masses $m_\chi \lesssim 1$ GeV discussed in this paper are smaller than the dark matter masses considered in [6] and hence these events are even safer from such experimental constraints.

B. Excited state decay

The decays of $\chi_e \rightarrow \chi_g + \gamma$ produce $\sim 2.5\text{--}3.5$ keV γ rays. These γ rays, which lie in the x-ray spectrum, can potentially be observed in detectors other than DAMA's. Indeed, unlike a conventional WIMP which deposits energy in a detector due to scattering between the WIMP and the nuclei in the detector, the decay of χ_e and the subsequent γ -ray energy release occurs in vacuum. This process can therefore be observed not just in a conventional dark matter detector which measures \sim keV energy depositions (where they appear as pure ionization energy and get classified as electron recoils), but also in any instrument which can observe events over a large *volume* even if the volume is a vacuum. In this section, we discuss current experimental bounds on such decays.

1. XENON100

The XENON100 Collaboration has released data from its preliminary run ~ 11.17 live days between October 20th to November 12th, 2009 [4]. In this run, the experiment recorded ~ 28 events identified as electron recoils in the energy band between $\sim 5\text{--}33$ keV nr. The observations were performed in a fiducial volume that was a cylinder with radius 13.5 cm and height 24.3 cm.

We now estimate the expected event rate in XENON100 as implied by the DAMA event rate. The actual event rate at DAMA is a function of the modulation fraction allowed by the underlying dark matter model. With a large modulation rate, the actual number of dark matter events at DAMA is decreased resulting in better agreement between DAMA and other experiments. Consequently, we parametrize the XENON100 constraints on this model as the minimal modulation fraction necessary for the two event rates to be consistent. We note that large modulation fractions $\sim 50\text{--}70\%$ are easy to obtain in this scenario since the initial excitation of χ_e requires inelastic, upscattering from χ_g (see Sec. II). In this scenario, the event rates at different experiments are related solely by the volumes of the two experiments. The other factor that affects the event rate is the time during which the observations were performed. XENON100 ran near the end of the month of October which is close to the trough of the DAMA modulation. This factor must be incorporated in the evaluation of the expected rate at XENON100.

The ~ 28 events of XENON100 are spread over a wide energy region, between $\sim 5\text{--}33$ keV nr. In this model, the decays of χ_e produce a sharp X-ray line at ~ 3 keV. But, this line is smeared by the energy resolution of XENON100. The detector response at these low energies is very poorly understood [23]. The energy resolution is measured above ~ 122 keV and these measurements are used to extrapolate the resolution at low energies [24]. In this paper, as described in Sec. II, we will use a Poisson distribution on the number of S1 photoelectrons which gives an energy resolution at ~ 3 keV as roughly ~ 1.14 keV. With these parameters, the constraint imposed by XENON100 on this parameter space is evaluated and the results are shown in Fig. 2 (see Sec. II for more details). These results indicate that the modulation fraction must be at least $\sim 50\%$.

We note that the limits derived in Fig. 2 may be conservative. The parameter space available for the model can be significantly bigger owing to several experimental uncertainties. For example, the energy resolution at 3 keV could be significantly worse than the above estimate as it is based upon an extrapolation by nearly 2 orders of magnitude where measurements have not been made. In this case, the events would be spread out more evenly in XENON100 making this scenario more consistent. Consequently, the DAMA signal can be fit with lower modulation fractions, opening up the parameter space.

In addition to ambiguities in the energy resolution of the detector, there is also uncertainty in the photoelectron yield of low-energy ~ 3 keV x rays in XENON100. The analysis of [4] was performed under the assumption that the photoelectron (PE) yield L_y of xenon was linearly proportional ($\propto 2.2 \frac{\text{PE}}{\text{keV}}$) to the x ray energy. However, these measurements were also made at ~ 122.5 keV [4]. It is unclear if this photoelectron yield remains linear at low energies.

If L_y was smaller, then the events would produce fewer photoelectrons and could appear in a region with a significantly smaller cut acceptance. In this case, there would be fewer expected events at XENON100, thereby opening up the parameter space of the model.

The above constraints were evaluated assuming that the signal in XENON100 was from a single ~ 3 keV line in the detector. However, the DAMA signal can also be fit through two spectral lines, one at around ~ 2.7 keV and another at ~ 4.7 keV (see Fig. 3). Indeed, these two spectral lines are actually a better fit to the DAMA data than a single line. In order to obtain two spectral lines instead of one, we need two excited states χ_{e_1} and χ_{e_2} that are split from the dark matter χ_g by ~ 2.7 keV and ~ 4.7 keV respectively. The existence of such states may be generic in UV completions of this framework, such as in composite dark matter models [25] and scenarios where the dark matter is charged under a broken non-Abelian group [26]. In this case, the events at XENON100 will not be clustered around ~ 10 keV, but would rather be more evenly spread across the region $\sim 5\text{--}25$ keV nr. Since there are significantly more events in this region, this also alleviates the constraints from XENON100 on this parameter space.

Despite these detector uncertainties, this model predicts that a significant fraction of events observed at XENON100 between $\sim 5\text{--}25$ keV nr are due to dark matter. Consequently, this model predicts that XENON100 will continue seeing such electron-recoil events in future runs of the experiment, and in fact even more during the summer. While the absence of such events will constrain this scenario, we note that the detector response at low energies has to be better understood before these constraints can be sharply imposed.

2. CDMS

The CDMS Collaboration has recently analyzed its low-energy electron-recoil spectrum in its germanium detector [27]. In order to facilitate a comparison between the event rates at CDMS and DAMA, this analysis assumed a Z^2 scaling in the scattering cross section. It was then found that the event rates in the two experiments would be

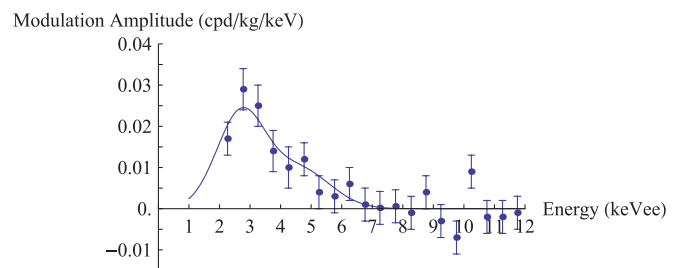


FIG. 3 (color online). A comparison of the predicted and observed spectra at DAMA for two lines, one at 2.7 keV and the other at 4.7 keV.

compatible if the dark matter signal modulated at $\sim 12\%$. In this scenario, the event rates at different experiments depend entirely on the volume of the detector. Comparing the relative volumes of the two detectors [2,27], we find that the event rate at CDMS is compatible with that of DAMA as long as the rate of dark matter induced electron recoils in DAMA is smaller than ~ 0.09 events/day/kg/keV. This implies that the observed annual modulation ~ 0.022 events/day/kg/keV in DAMA can be reproduced if the dark matter signal modulates at $\sim 24\%$. This large modulation fraction is quite easy to achieve in the scenario discussed in this paper since the initial excitation of χ_e requires inelastic, upscattering from χ_g (see Sec. II).

We note that since these events are visible at CDMS, this scenario can be strongly constrained if the CDMS Collaboration analyzes the annual modulation of its electron-recoil events. In this model, the annual modulation signal at DAMA implies a modulation of ~ 0.015 events/day/kg/keV at CDMS. The nonobservation of such a modulation will rule out this scenario as an explanation for the DAMA result.

3. CoGeNT

The CoGeNT Collaboration has released its observed recoil spectrum, consisting of both electron- and nuclear-recoil events [28]. This experiment observed an event rate of at least ~ 1.8 events/kg/day/keVee (prior to efficiency corrections). Assuming at least a 24% modulation in the event rate at DAMA (see Sec. III B 2) and scaling the expected event rates between the two experiments using the relative volume of the apparatus, we find that the DAMA result implies a rate ~ 0.06 events/kg/day/keVee at CoGeNT. This is of course smaller than the rate observed at CoGeNT and is hence not a constraint. However, with sufficient exposure, the 3 keVee line produced by the decays of χ_e may be observable at CoGeNT. Furthermore, just like CDMS, an analysis by CoGeNT of the annual modulation of its signal could constrain this scenario.

4. CAST

The decay of $\chi_e \rightarrow \chi_g + \gamma$ occurs in vacuum and is visible in any volume that is instrumented to observe ~ 2.5 – 3.5 keV γ rays. The CAST experiment [29], constructed to search for solar axions, is an example of such an instrumented vacuum region that is sensitive to x rays. The experiment consists of two parallel pipes of cross-sectional area 14.5 cm² and length 10 m [29]. Detectors are placed at the ends of the pipes and are sensitive to x rays in the keV regime. CAST aims to look for solar axions by looking at the variation in the observed γ -ray count as the telescope's orientation with respect to the Sun is changed. In this scenario, the decays of χ_e give rise to a constant background γ flux at CAST. This background flux is $\sim 4.32 \frac{\text{events}}{\text{cm}^2 \text{ day keV}}$ [29]. Assuming at least a 24% annual

modulation in DAMA (see Sec. III B 2), the event rate from χ_e decay is no greater than $\sim 3 \times 10^{-4} \frac{\text{events}}{\text{cm}^3 \text{ day keV}}$ in the CAST volume. Accounting for the γ rays that are oriented toward the detectors at the end of the telescope, we find that the expected flux from χ_e decays is $\lesssim 0.01 \frac{\text{events}}{\text{cm}^2 \text{ day keV}}$, significantly smaller than the observed background.

5. Bubble chamber experiments

Bubble chamber experiments such as COUPP [30] and PICASSO [31] are capable of operating at low thresholds. In particular, COUPP has run with a threshold ~ 5 keV, while PICASSO has operated above ~ 2 keV. However, these experiments are intrinsically insensitive to electron and photon energy deposition below ~ 350 keV [30,31] and do not constrain the decays of χ_e . Moreover, the initial upscattering of the dark matter χ_g occurs at energies below ~ 1 keV for the parameter space considered in Sec. II. This energy is below the threshold of these experiments and is thus unconstrained.

6. Near-Earth x-ray emission

The dark matter χ_g can be upscattered to χ_e from the Earth, the Moon, and the Sun. The decays of the excited state χ_e produces γ rays which can be detected by x-ray telescopes. The Sun is a powerful source of x rays and the contribution of the dark matter to the solar x-ray flux is negligible in this scenario. Moreover, during the day, the solar x-ray flux illuminates the Earth and the Moon, resulting in significant x-ray emission from them [32]. However, at night, these objects are significantly darker in the x-ray spectrum and we will use x-ray measurements of this flux to constrain this scenario. We consider three kinds of measurements.

First, satellites in low Earth orbit such as RTXE [33] and SWIFT [20], with orbits ~ 600 km, have measured the cosmic x-ray background from the dark side of the Earth. In these measurements, the satellite is behind the Earth, with its telescope facing the open cosmos. The telescope view is restricted to be at least 30° away from the Earth horizon in order to avoid backgrounds from the sunlit portion of the Earth [20]. These satellites are therefore sensitive to decays of χ_e that occur anywhere within the telescope field of view that lies beyond the orbit of the satellite. The decaying $\chi_e \rightarrow \chi_g + \gamma$ produces a ~ 3 keV x-ray line and the flux from these decays must be consistent with the measured cosmic x-ray background. Using the instrumental energy resolution ~ 0.1 keV of SWIFT, we require that the flux from the decaying χ_e at a ~ 600 km orbiting satellite be no greater than $\sim 0.03 \frac{\text{cts}}{\text{cm}^2 \text{ s sr}}$ in the energy bin around ~ 3 keV [20].

The flux of x rays at a local experiment from the decaying χ_e can be calculated as follows. The initial upscattering of the dark matter χ_g occurs with a roughly uniform cross section in the Earth, giving rise to a uniform density of χ_e

inside the Earth. Away from the Earth, at a distance r from the center of the Earth, the density of χ_e drops $\propto r^{-2}$. Ultimately, this density extends out to a distance $L \sim \frac{v_f}{\Gamma}$ set by the decay length of χ_e (see Sec. II), after which the density is exponentially cut off. The x rays produced in χ_e decays in this entire region can strike the telescope and hence the total x-ray flux is computed by integrating over the decays that occur in this entire region.

In this scenario, the density of χ_e inside the Earth is set by the event rate required to fit DAMA. The only other essential parameter that determines the flux in an orbiting telescope is the decay length of χ_e . For a decay length significantly smaller than the Earth radius, the density of χ_e drops exponentially away from the Earth. In this case, the density of χ_e in the region that lies beyond a telescope that is on a ~ 600 km orbit is suppressed compared to the density of χ_e in DAMA, leading to a reduction in the x-ray flux at the telescope. Performing the above calculations numerically, we find that the flux from the decays of χ_e are smaller than the observed cosmic x-ray background at an x-ray telescope orbiting the Earth at ~ 600 km if the decay length of χ_e is smaller than ~ 1000 km (assuming that the DAMA modulation fraction is $\sim 50\%$). With this choice of decay length, this scenario is consistent with the observations of the cosmic x-ray background by low Earth orbit satellites such as RTXE [33] and SWIFT [20].

Second, the RTXE satellite pointed its telescope at the dark side of the Earth and measured the x-ray flux emerging from it. The collaboration assumed that the x-ray flux from this region was entirely due to instrumental systematics, and subsequently subtracted this flux from its measurements of the clean x-ray sky to get a systematics free measurement of the cosmic x-ray background [33]. In this measurement, it was found that the x-ray flux emerging from the dark side of the Earth was comparable to the cosmic x-ray background. Numerically evaluating this contribution, we find that the x-ray flux at RTXE is consistent with the measured background count rate in the ~ 3 keV bin as long as the decay length of χ_e is smaller than ~ 900 km.

Finally, the Chandra x-ray telescope measured the flux of x rays emerging from the dark side of the Moon [34]. This measurement was performed with the telescope pointed toward the dark side of the Moon. Chandra is therefore sensitive to the decays of χ_e that occur between its orbit and the lunar surface. There are two sources of χ_e in this region. First, upscattering from the Earth creates a local flux of χ_e in the region near the Earth. However, since the decay length of χ_e must be smaller than ~ 900 – 1000 km due to the preceding considerations, the flux of χ_e that lies beyond the perigee ~ 16000 km of Chandra is negligible and does not constrain this scenario. Second, the dark matter χ_g can get upscattered in the Moon and then subsequently decay above the lunar surface. These x rays would then be visible to Chandra. However,

with the parameters chosen in this model, the flux of x rays at Chandra produced by the dark side of the Moon are significantly smaller than the measurements of Chandra.

In summary, near-Earth measurements of the local x-ray flux can impose significant constraints on the parameter space of this scenario. Consistency with these measurements requires that the decay length of the excited state χ_e be smaller than ~ 1000 km. This is the biggest constraint in achieving this scenario through an electric dipole moment (EDM) operator instead of the magnetic dipole operator (1) considered in this paper. In the case of an EDM operator, the scattering cross section for $\chi_g \rightarrow \chi_e$ is enhanced by $\frac{1}{v^2}$ [35]. In order to match the event rate at DAMA, the initial upscattering rate can be made sufficiently small by taking the scale suppressing the EDM operator to be significantly higher than the scale used in (1). But, in this case, the decay length of the dark matter also increases and, in particular, becomes larger than the Earth radius resulting in a conflict with the above x-ray bounds.

For the magnetic dipole moment operator (1) considered in this paper, there is a significant parameter space where the DAMA signal can be fit with the excited state decay length being shorter than ~ 1000 km. The decay lengths are ~ 100 – 1000 km in the parameter space available to this model after the imposition of constraints from XENON100 (see Sec. II and Fig. 2). These decay lengths were computed using the χ_e lifetime (7) and integrating over a distribution of final state velocities of the χ_e produced after the upscattering of χ_g . We note that toward the lower end of this parameter space, when the decay lengths become smaller than ~ 100 km, these x-ray constraints entirely vanish since the decays are confined to the lower atmosphere which absorbs ~ 3 keV x rays well before they can make it out to the orbits of X-ray satellites.

7. X-ray line emission

Collisions with interstellar gas can upscatter the dark matter χ_g to χ_e in the Galaxy. The subsequent decay of χ_e produces a ~ 3 keV x-ray line that contributes to the Galactic x-ray background. Line emissions from decaying dark matter in this energy band were searched for in [36] and an upper bound $\sim 10^{27}$ s was placed on the dark matter lifetime for dark matter masses in the keV regime. For GeV dark matter producing keV lines, this bound is weakened to a lifetime of $\sim 10^{21}$ s since the number density of a GeV mass dark matter particle is smaller than that of a keV dark matter particle by 10^{-6} . In our scenario, this bound translates into a bound on the Galactic upscattering rate. Most of the Galaxy consists of hydrogen gas which has an average number density of ~ 1 cm $^{-3}$ in the Galactic disk. With this gas density, the upscattering rate is smaller than 10^{-21} s $^{-1}$ as long as the χ_g upscattering cross section is smaller than $\sim 10^{-28}$ cm 2 . Similar bounds were also placed in [37].

The upscattering cross sections considered in this scenario are considerably smaller than the above limit.

The typical scattering cross section considered in this model is provided by (5) which yields per-nucleon scattering cross sections $\sim 10^{-36}\text{--}10^{-38}$ cm² in the Earth. But, this scattering cross section is between the magnetic dipole of the dark matter χ_g and the charge of the nucleus. As explained in Sec. II, this is the relevant scattering cross section in this scenario since most of the Earth is made up of nuclei that have no net spin. However, when there is a nuclear spin, there is an additional scattering process provided by the interaction between the magnetic dipole moments of the dark matter and the nucleus itself [14,38]. For the case of hydrogen, this dipole-dipole scattering cross section is larger by a factor of ~ 4 [14,38]. Consequently, this model would imply upscattering cross sections $\sim 10^{-35}\text{--}10^{-37}$ cm² in the Galaxy between the dark matter and hydrogen, which is smaller than the limit imposed by [36].

8. Directional detection of dark matter

Significant progress has been recently achieved in constructing detectors that are sensitive to the direction of the incoming dark matter particles. Conventional inelastic dark matter models that cause nuclear energy deposition give rise to daily modulations in the direction of the dark matter signal in these experiments [39]. But, in this case, the decay of χ_e emits a photon isotropically and hence the direction of the dark matter signal will not modulate.

These experiments can nevertheless serve as powerful probes of luminous dark matter since they are large volume detectors.⁷ Current runs of these experiments do not constrain this scenario since they were operated at high thresholds (for example, NewAge [40] and DRIFT-2 [41]). DMTPC [42] has also published results of its initial run, with its cuts optimized to search for events at high recoil energies. Luminous dark matter will give rise to visible signals in these experiments if they can be operated at a threshold below ~ 3 keV with reduced backgrounds at these energies.

9. Neutrino detectors

Neutrino detectors like Borexino [43] and Super-Kamiokande [44] are large volume detectors. However, their operating thresholds are close to ~ 1 MeV and hence these experiments are insensitive to luminous dark matter.

C. Collider, astrophysical, and CMB constraints

Collider and other precision particle physics limits on light dark matter particles with magnetic moments were considered by [35]. The most stringent of these limits arise from direct production of dark matter particles in the

Tevatron. As per this analysis, dark matter particles with magnetic moments $\sim 10^{-17}$ e-cm $\sim (\text{TeV})^{-1}$ are safe from collider constraints. This is roughly the size of the magnetic moments considered in this paper (see Sec. II). Moreover, as pointed out in [35], magnetic moments larger than the above limit are also allowed if the magnetic moment operator falls apart at Tevatron energies. Indeed, if this operator is radiatively generated by weak scale $\mathcal{O}(100 \text{ GeV})$ particles (see Sec. II), it would fall apart at the scale of those particles. For example, if the operator falls apart at LEP energies, the dipole moment has to be smaller than $(1 \text{ TeV})^{-1}$ [45]. The parameter space considered in this paper satisfies this constraint.

Astrophysical limits on dark matter interaction cross sections with nuclei have also been placed. The most significant of these constraints arise from the capture and subsequent annihilation of dark matter into neutrinos. These are then constrained by measurements at Super-Kamiokande [44,46–48]. Similarly, it has also been pointed out that the capture of dark matter in white dwarfs located in globular clusters with dark matter densities greater than ~ 1000 times the mean Galactic dark matter density could also place limits on the dark matter-nucleon interaction cross section [49,50]. However, both these bounds are model-dependent and can be easily overcome with variations of the underlying particle physics model [6]. A parameter space similar to the one considered in this paper was discussed in [6] and we refer the reader to the discussion in [6] on the applicability of these bounds.

The cosmic microwave background (CMB) also constrains light dark matter [51] that annihilates to electromagnetic and colored standard model particles with a thermal annihilation cross section. In fact, dark matter masses below ~ 10 GeV are in conflict with WMAP5 observations if the dark matter dominantly annihilates to the above final states. In this model, this constraint can be naturally evaded. The magnetic dipole moment operator (1) connects two different states χ_g and χ_e , but vanishes by fermion anticommutation when the two states are identical. During freeze-out, the states χ_g and χ_e are present in the plasma since they have nearly identical masses. The operator (1) then causes annihilations between these states and the standard model. For the parameters chosen in Sec. II, this cross section is roughly the thermal relic cross section necessary to generate a dark matter abundance of χ_g and χ_e (see Fig. 2). χ_e then decays rapidly (well before nucleosynthesis) to χ_g through (1), resulting in a relic population of χ_g . In order for (1) to induce annihilations of χ_g , the state χ_e has to be integrated out of the theory. This results in a dimension-7 operator that mediates the annihilation of χ_g into two photons, suppressed by two powers of the dipole moment scale Λ and one power of the dark matter mass. These annihilation cross sections are significantly suppressed compared to the thermal relic annihilation cross section between χ_g and χ_e since the

⁷We thank Neal Weiner for pointing this out to us.

latter are mediated by a dimension-5 operator suppressed by only one power of Λ . Consequently, at the effective theory level, this model is intrinsically safe from CMB constraints on light dark matter. UV completions of this operator must however not open significant annihilation channels into charged or colored standard model particles.

IV. CONCLUSIONS

We have proposed a novel explanation for the DAMA result arising from the excitation of dark matter in the Earth followed by the decay of the excited state through single photon emission. When the decay occurs inside a direct detection experiment it appears as electromagnetic, not nuclear, energy deposition. This naturally avoids many of the constraints from direct detection experiments. Both the upscattering and the decay, as well as possibly the relic abundance, are set by a single operator, the dipole moment operator. Thus it is a tightly determined model from the beginning, with essentially only two free parameters, the dark matter mass and the scale suppressing the dipole moment operator. Interestingly, for reasonable choices of both parameters, a mass ~ 1 GeV and a scale ~ 1 TeV, this model can explain the DAMA result and avoid all other constraints. In particular, this model naturally has a higher annihilation cross section in the early Universe when both states exist and a much lower cross section occurs after the excited state population has decayed. Thus the annihilation cross section drops significantly after freeze-out, allowing the model to have the correct relic abundance but to avoid the tight CMB constraints on light dark matter.

Unlike every other direct detection model, in this case the actual detector material is irrelevant. The observed rate of events will only be proportional to the volume of the detector, not its mass or composition. Experiments such as CDMS and XENON100 could see a signal of this model if

they have sensitivity to low-energy, $\lesssim 3$ keV, electronic events. In fact, current results from XENON100 provide one of the strongest constraints on this model. These experiments should see an annual modulation precisely proportional to DAMA's signal and the ratio of the volumes of the two experiments. Such a signal should be clearly visible at XENON100 and CDMS if they measure the annual modulation of their electronic events. Note that in this case a directional detection experiment will actually not reveal additional information since the decay of the dark matter emits the photon isotropically. On the other hand, because the cross section for the original upscattering of the dark matter in the Earth does have angular dependence, there can be an observable daily modulation of the signal. As the angle of the dark matter wind hitting the Earth near DAMA changes over the course of the day, the rate DAMA sees will also vary. Given the high statistical significance of DAMA's signal, this daily modulation may also be visible if DAMA were to search for it in their data. Over most of our parameter space, however, this daily modulation is suppressed because the initial upscattering of the dark matter off a nucleus in the Earth is not strongly peaked in the forward direction. This is partly because the dark matter is lighter than the nucleus and so can easily backscatter. Nevertheless, this may make an interesting signal to search for.

ACKNOWLEDGMENTS

We would like to thank Sergei Dubovsky, Roni Harnik, Kiel Howe, Dan McKinsey, Kaixuan Ni, Prashant Saraswat, Martin Schmaltz, Peter Sorensen, Jesse Thaler, and Neal Weiner for useful discussions. B. F. is supported by DOE Grant No. DE-FG02-01ER-40676. S. R. is supported by the DOE Office of Nuclear Physics under Grant No. DE-FG02-94ER40818. S. R. is also supported by NSF Grant No. PHY-0600465.

-
- [1] R. Bernabei *et al.*, *Eur. Phys. J. C* **67**, 39 (2010).
 - [2] R. Bernabei *et al.* (DAMA Collaboration), *Eur. Phys. J. C* **56**, 333 (2008).
 - [3] Z. Ahmed *et al.* (CDMS-II Collaboration), *Science* **327**, 1619 (2010).
 - [4] E. Aprile *et al.* (XENON100 Collaboration), *Phys. Rev. Lett.* **105**, 131302 (2010).
 - [5] D. Tucker-Smith and N. Weiner, *Phys. Rev. D* **64**, 043502 (2001).
 - [6] P. W. Graham, R. Harnik, S. Rajendran, and P. Saraswat, *Phys. Rev. D* **82**, 063512 (2010).
 - [7] B. Feldstein, A. L. Fitzpatrick, E. Katz *et al.*, *J. Cosmol. Astropart. Phys.* **03** (2010) 029.
 - [8] B. Feldstein, A. L. Fitzpatrick, and E. Katz, *J. Cosmol. Astropart. Phys.* **01** (2010) 020.
 - [9] S. Chang, A. Pierce, and N. Weiner, *J. Cosmol. Astropart. Phys.* **01** (2010) 006.
 - [10] Y. Bai and P. J. Fox, *J. High Energy Phys.* **11** (2009) 052.
 - [11] A. Bottino, F. Donato, N. Fornengo, and S. Scopel, *Phys. Rev. D* **69**, 037302 (2004).
 - [12] F. Petriello and K. M. Zurek, *J. High Energy Phys.* **09** (2008) 047.
 - [13] C. Savage, G. Gelmini, P. Gondolo, and K. Freese, *J. Cosmol. Astropart. Phys.* **04** (2009) 010.
 - [14] S. Chang, N. Weiner, and I. Yavin, [arXiv:1007.4200](https://arxiv.org/abs/1007.4200).
 - [15] A. L. Fitzpatrick and K. M. Zurek, [arXiv:1007.5325](https://arxiv.org/abs/1007.5325).
 - [16] T. Banks, J. F. Fortin, and S. Thomas, [arXiv:1007.5515](https://arxiv.org/abs/1007.5515).
 - [17] J. Kopp, V. Niro, T. Schwetz, and J. Zupan, *Phys. Rev. D* **80**, 083502 (2009).

- [18] M. Pospelov, A. Ritz, and M. B. Voloshin, *Phys. Rev. D* **78**, 115012 (2008).
- [19] R. Bernabei *et al.* (DAMA Collaboration), *Nucl. Instrum. Methods Phys. Res., Sect. A* **592**, 297 (2008).
- [20] A. Moretti *et al.*, *AIP Conf. Proc.* **1126**, 223 (2009).
- [21] H. Chisholm, Crust (Geology), [http://en.wikipedia.org/wiki/Crust_\(geology\)](http://en.wikipedia.org/wiki/Crust_(geology)).
- [22] Kaixuan Ni (private communication).
- [23] P. Sorensen, [arXiv:1007.3549](https://arxiv.org/abs/1007.3549).
- [24] E. Pantic, Response of the XENON100 Detector to Gamma and Neutron Radioactive Sources, http://xenon.astro.columbia.edu/talks/pantic_ucla_dm2010.pdf.
- [25] D. S. M. Alves, S. R. Behbahani, P. Schuster, and J. G. Wacker, *Phys. Lett. B* **692**, 323 (2010).
- [26] N. Arkani-Hamed, D. P. Finkbeiner, T. R. Slatyer, and N. Weiner, *Phys. Rev. D* **79**, 015014 (2009).
- [27] Z. Ahmed *et al.* (CDMS Collaboration), *Phys. Rev. D* **81**, 042002 (2010).
- [28] C. E. Aalseth *et al.* (CoGeNT Collaboration), [arXiv:1002.4703](https://arxiv.org/abs/1002.4703).
- [29] I. G. Irastorza *et al.*, in *Proceedings of International Symposium on Detector Development for Particle, Astroparticle and Synchrotron Radiation Experiments, SNIC 2006, Menlo Park, California, 2006* (SLAC, Palo Alto, 2006), p. 0036.
- [30] E. Behnke *et al.* (COUPP Collaboration), *Science* **319**, 933 (2008).
- [31] S. Archambault *et al.*, *Phys. Lett. B* **682**, 185 (2009).
- [32] A. Bhardwaj, [arXiv:astro-ph/0209107](https://arxiv.org/abs/astro-ph/0209107).
- [33] M. Revnivtsev, M. Gilfanov, R. Sunyaev, K. Jahoda, and C. Markwardt, *Astron. Astrophys.* **411**, 329 (2003).
- [34] B. J. Wargelin, M. Markevitch, M. Juda, V. Kharchenko, R. J. Edgar, and A. Dalgarno, *Astrophys. J.* **607**, 596 (2004).
- [35] K. Sigurdson, M. Doran, A. Kurylov *et al.*, *Phys. Rev. D* **70**, 083501 (2004).
- [36] A. Boyarsky, J. Nevalainen, and O. Ruchayskiy, *Astron. Astrophys.* **471**, 51 (2007).
- [37] S. Profumo and K. Sigurdson, *Phys. Rev. D* **75**, 023521 (2007).
- [38] V. Barger, W. Y. Keung, and D. Marfatia, [arXiv:1007.4345](https://arxiv.org/abs/1007.4345).
- [39] D. P. Finkbeiner, T. Lin, and N. Weiner, *Phys. Rev. D* **80**, 115008 (2009).
- [40] K. Miuchi *et al.*, *Phys. Lett. B* **686**, 11 (2010).
- [41] S. Burgos *et al.*, *Astropart. Phys.* **28**, 409 (2007).
- [42] S. Ahlen *et al.*, [arXiv:1006.2928](https://arxiv.org/abs/1006.2928).
- [43] M. Leung, Ph.D. thesis, Princeton University, 2006, http://borex.princeton.edu/public-docs/theses/leung_phd_by_chapter/leung_phd_0_front_matter.pdf.
- [44] S. Desai *et al.* (Super-Kamiokande Collaboration), *Phys. Rev. D* **70**, 083523 (2004); **70**, 109901(E) (2004).
- [45] E. Masso, S. Mohanty, and S. Rao, *Phys. Rev. D* **80**, 036009 (2009).
- [46] D. Hooper, F. Petriello, K. M. Zurek, and M. Kamionkowski, *Phys. Rev. D* **79**, 015010 (2009).
- [47] K. Griest and D. Seckel, *Nucl. Phys.* **B283**, 681 (1987).
- [48] A. Gould, *Astrophys. J.* **321**, 560 (1987).
- [49] M. McCullough and M. Fairbairn, *Phys. Rev. D* **81**, 083520 (2010).
- [50] D. Hooper, D. Spolyar, A. Vallinotto, and N. Y. Gnedin, *Phys. Rev. D* **81**, 103531 (2010).
- [51] S. Galli, F. Iocco, G. Bertone *et al.*, *Phys. Rev. D* **80**, 023505 (2009).